Density Functional Theory Calculations of Hydrogen-Containing Defects in Forsterite, Periclase, and α-Quartz

Nora H. de Leeuw*

Department of Chemistry, University of Reading, Whiteknights, Reading RG6 6AD, United Kingdom

Received: March 15, 2001; In Final Form: August 2, 2001

Electronic structure calculations using the density functional theory within the generalized-gradient approximation and ultra-soft pseudopotentials have been used to investigate the absorption of water and protons in forsterite (Mg_2SiO_4), periclase (MgO), and α-quartz (α-SiO_2). The calculated structural parameters are found to be in good agreement with experiment. Absorption of water in the perfect lattice is calculated to be an endothermic process in all three minerals but exothermic when associatively adsorbed at the forsterite {010} surface. The introduction of cation vacancies in the lattices is energetically unfavorable, more so for the formation of a silicon vacancy than a magnesium vacancy. The process of introducing a neutral silicon vacancy in the lattice, by reaction of a silicon atom with gaseous oxygen to form SiO_2, is endothermic by approximately the same amount of energy (approximately 430 kJ mol^{-1}) in both quartz and forsterite, but introducing an equivalent magnesium vacancy in the periclase lattice is less endothermic (163 kJ mol^{-1}) than the same process in forsterite (217 kJ mol^{-1}). Absorption of hydrogen molecules at the vacant cation sites is a highly exothermic process, releasing on average between 213 and 273 kJ mol^{-1} per proton when absorbed at a magnesium vacancy and approximately 275 kJ mol^{-1} per proton at a vacant silicon site. When we calculate the replacement of MgO and SiO_2 units by liquid water molecules, as a first step in the process of dissolution of the minerals, we find that it is an endothermic process in the bulk minerals but exothermic by 71 kJ mol^{-1} for replacing an MgO unit at the forsterite {010} surface.

Introduction

Forsterite is the magnesium end member of the common rock-forming mineral group of olivines. Olivines are extensively found in the Earth's mantle and are generally richer in magnesium than in iron.[1] The mineral can be synthesized by solid-state reactions between MgO and SiO_2 at elevated temperatures (1100−1400 °C) and from stoichiometric mixtures in solution at low temperature (500 °C).[2] Because of their prominence as mantle materials, forsterite and olivines in general have been the subject of much research, both experimental and theoretical. The emphasis of many investigations has naturally been on the mineral's behavior at high pressures and temperatures, e.g., the determination of high-pressure and high-temperature thermodynamic data[3] and the transition mechanism of olivine to high-pressure polymorphs.[4] Other recent investigations have included trace element partitioning[5,6] and grain boundary melting.[7,8]

Quartz is one of the most abundant minerals and occurs as an essential constituent of many igneous, sedimentary, and metamorphic rocks.[9] α-Quartz is the stable form at ambient pressures and temperatures up to 573 °C, and we have therefore concentrated on this structure. In addition to the geological importance of the natural quartz mineral and because of its high-frequency stability, synthetic quartz crystals are used in high-frequency devices[10,11] and in cellular and satellite network applications.[12] This need for high-grade synthetic quartz crystals has sparked off many studies into factors affecting crystal growth and defect formation.[13−16]

Natural periclase, present in the lower mantle, is formed at relatively high temperatures from the metamorphism of dolomites ($MgCa(CO_3)_2$) and magnesian limestones and may contain up to 5−10% FeO and traces of zinc and possibly manganese.[9] Periclase is a very stable material, readily synthesized from $MgCl_2$ or $Mg(OH)_2$,[17] and is important both as a support for metal catalysts and high-temperature superconductors[18] and as a catalyst in its own right.[19,20] Because of these applications and its simple structure, MgO has been the subject of much research, both experimentally, for example,[21−24] and theoretically, for example.[25−28] Although DFT techniques have been widely used to study MgO, these have concentrated on the surface structures of the material, for example,[29,30] and/or surface adsorption behavior, for example.[31−34]

Of particular interest is the influence of water in these minerals, which has a profound effect on physical properties such as diffusion rates, crystal strength (hydrolytic weakening), and melting point.[35−37] In forsterite, for example, the melting point (1890 °C) increases with pressure under anhydrous conditions to approximately 2030 °C at a pressure of 30 kbar but decreases with pressure under water-saturated conditions to 1400 °C at the same pressure.[9] Water is present in significant quantities both in the forsterite bulk crystal and at grain boundaries, often incorporated as OH clusters at cation defect sites.[38] Similarly, considerable amounts of water are found in α-quartz, and the interaction of water with silica has been the subject of a wide range of investigations, both experimental studies, such as the investigation of the role of water in controlling crack velocity in α-quartz single crystals[36] and theoretical work, such as local density functional (LDF) calculations of the hydrogarnet defect in quartz,[39] ab initio

* To whom correspondence should be addressed. E-mail: n.h.deleeuw@reading.ac.uk.

10.1021/jp0109978 CCC: $20.00 © 2001 American Chemical Society
Published on Web 09/12/2001

TABLE 1: Total Energy of Bulk Forsterite as a Function of Plane-Wave Cutoff and Density of *k*-Point Sampling

	E_{total} of bulk forsterite (eV)				
k-point mesh	$E_{cut} = 300$ eV	$E_{cut} = 400$ eV	$E_{cut} = 500$ eV	$E_{cut} = 600$ eV	$E_{cut} = 700$ eV
$2 \times 2 \times 2$			−193.827 165	−193.841 662	
$3 \times 3 \times 3$	−193.634 157	−193.700 079	−193.792 986	−193.807 573	−193.815 053
$4 \times 4 \times 4$			−193.795 394	−193.809 382	

calculations of $(OH)_4$ defects and interstitial water molecules in quartz,[40,41] and the first detailed studies of interstitial diffusion of water in quartz using CNDO self-consistent molecular orbital methods[42] and a classical interatomic potential approach.[35]

In this paper, we present results of electronic structure calculations of the incorporation of protons and water in the bulk crystal of forsterite (Mg_2SiO_4) and for comparison calculate the same processes in periclase (MgO) and α-quartz (SiO_2), using identical simulation parameters. Catlow and co-workers pioneered the calculation of defects in forsterite, using interatomic potential methods.[37,43] However, the defect energies calculated by these simpler methods for the incorporation of water into the mineral were found to be rather large. More recently, Brodholt and Refson[44] investigated the introduction of pairs of vacancies into the forsterite crystal and successive protonation of these vacancies by interstitial hydrogen atoms. We were, however, interested in calculating the formation energy of single vacancy sites, rather than vacancy pairs, and comparing forsterite with MgO and SiO_2 to investigate whether the presence of both types of oxides in one structure affects the defect formation energies compared to the pure oxides. In this work, we therefore investigate the absorption of water, both interstitially in the perfect lattice and at Mg and Si defect sites. To this end, we calculate the introduction of magnesium and silicon defect sites in the forsterite crystal and compare the energies of these processes with the equivalent process in both periclase and α-quartz. We then investigate the introduction of protons at the different vacancy sites in all three minerals and finally study the adsorption of water at the forsterite {010} surface, which is both experimentally[9] and theoretically[45,46] found to be the main cleavage plane of forsterite.

Computational Methods

The total energy and structure of the systems were determined using the Vienna ab Initio Simulation Program (VASP),[47−50] employing ultra-soft "Vanderbilt"-like pseudopotentials[51,52] which allow a smaller basis set for a given accuracy. The basic concepts of density functional theory (DFT) and the principles of applying DFT to pseudopotential plane-wave calculations has been extensively reviewed elsewhere[53−55] and DFT calculations have been performed on a wide range of applications, from metals, for example,[56] to ionic solids, for example,[44,57] including surface studies and adsorbates, for example.[58] Within the pseudopotential approach, only the valence electrons are treated explicitly and the pseudopotential represents the effective interaction of the valence electrons with the atomic cores. The valence orbitals are represented by a plane-wave basis set, in which the energy of the plane waves is less than a given cutoff (E_{cut}). The magnitude of E_{cut} required to converge the total energy of the system has important implications for the size of the calculation when studying elements such as oxygen, which has tightly bound 2p electrons. In our calculations, the cores consisted of orbitals up to and including the 1s orbital for oxygen, the 2s orbital for Mg, and the 2p orbital for Si. The calculations were performed within the generalized-gradient approximation (GGA), using the exchange-correlation potential developed by Perdew and Wang.[59] The degree of convergence of the total energy depends on a number of factors, two of which are the plane-wave cutoff and the density of *k*-point sampling within the Brillouin zone. We have investigated these by undertaking a number of calculations for forsterite, the most complex of the three materials, with different values for these parameters (Table 1), and by means of these test calculations, we have determined values for E_{cut} (600 eV) and the size of the Monkhorst-Pack[60] *k*-point mesh ($3 \times 3 \times 3$), so that the total energy is converged to within 0.01 eV (<0.004%). The optimization of the atomic coordinates (and unit cell size/shape for the bulk materials) was performed via a conjugate gradients technique which utilizes the total energy and the Hellmann−Feynman forces on the atoms (and stresses on the unit cell). As we compare the uptake of interstitial water molecules, cation defect formation and subsequent formation of OH clusters in forsterite with the equivalent processes in the structures made up of its constituent substances, MgO (in the form of periclase) and SiO_2 (as α-quartz), we have used identical parameters in our calculations of the different processes in the three materials.

For modeling the forsterite {010} surface, we used the usual approach for modeling surfaces, using three-dimensional periodic boundary conditions by considering a slab of forsterite. The surface simulation cell was 10.2 Å thick with a vacuum layer of approximately 20 Å between the images of the unhydrated surfaces and at least 15 Å between the images of the hydrated surfaces. In earlier work on CaO and CaF_2 surfaces, we showed, by means of calculating a series of various slab thicknesses and gap widths, that even a slab thickness of 8 Å and gap width of 10 Å were sufficient for the surface calculations to be convergent with respect to surface energy to within 0.001 Jm^{-2} (<0.2%).[58] Furthermore, calculations on the reactants and products were on equivalent supercells to achieve cancellation of basis set errors (this included calculations on the isolated H_2, O_2, and water molecules).[32]

When defects, such as vacancies, interstitials or surfaces, were introduced, the cell parameters were kept at the relaxed values obtained for the perfect crystal lattice, although the atoms within the simulation cells were allowed to move in response to the introduction of the defects, thereby ensuring short-range relaxation of the lattice. By keeping the lattice parameters fixed at the optimized structures of the perfect bulk materials and the simulation cells charge neutral, interactions between defects were kept to a minimum, which ensured as far as possible that we modeled the effect of low concentrations of water uptake and OH formation, rather than unrealistically large defect concentrations.

Results and Discussion

Forsterite has an orthorhombic structure with spacegroup *Pbnm*, $a = 4.7560$ Å, $b = 10.2070$ Å, $c = 5.9800$ Å, and $\alpha = \beta = \gamma = 90°$.[61] Its crystal structure comprises SiO_4 tetrahedra linked by magnesium cations in two distinct octahedral sites, M1 or M2, where M2 is the larger, more symmetric site. The calculated lattice vectors have expanded by about 0.5% from the experimental structure. α-Quartz has a hexagonal structure with spacegroup $P3_121$. The silicon atoms are four-coordinated in a tetrahedral arrangement by oxygen atoms, which form

TABLE 2: Comparison of Calculated and Experimental Structural Parameters of Forsterite, α-Quartz, and Periclase

calculated and experimental properties of forsterite, α-quartz, and Periclase						
	Mg_2SiO_4		α-SiO_2		MgO	
properties	exp.	calc.	exp.	calc.	exp.	calc.
volume (Å^3)	290.30	295.82	112.95	121.77	74.99	76.24
a (Å)	4.756	4.781	4.913	5.044	4.212	4.240
b (Å)	10.207	10.297	4.913	5.044	4.212	4.240
c (Å)	5.980	6.011	5.404	5.527	4.212	4.240
α (degrees)	90	90	90	90	90	90
β (degrees)	90	90	90	90	90	90
γ (degrees)	90	90	120	120	90	90

bridges between two silicons. We used a unit cell of $a = b = 4.913$ Å and $c = 5.404$ Å and $\alpha = \beta = 90°$ and $\gamma = 120°$,[9] which upon electronic and ionic minimization became expanded by approximately 2.5%, somewhat more than previous DFT calculations of α-quartz, due to the fact that the planewave energy cutoff and number of *k* points in this work were optimalised for the forsterite structure. For example, calculated lattice parameters for α-quartz are reported for *a* between 4.876 and 4.954 Å and *c* between 5.490 and 5.441 Å.[62−64] Finally, MgO has the rock-salt structure, spacegroup *Fm*3*m*, and in the bulk, each magnesium and oxygen ion is six-coordinate.[9] Perfect crystals show a cubic morphology with $a = b = c = 4.212$ Å and $\alpha = \beta = \gamma = 90°$. Our calculated lattice parameters, which expanded by about 0.7% from the experimental structure, are also in good agreement with previous calculations of MgO lattice parameters. For example, Refson et al.[32] calculated a lattice parameter of 4.217 Å using DFT calculations within the local density approximation (LDA), whereas Königstein et al.[65] used periodic Hartree−Fock calculations to obtain lattice parameters of 4.203 Å. In Table 2, the experimental and calculated structural properties of the three minerals are compared, from which it is clear that the calculated parameters are in adequate agreement with the experimental structures.

Figure 1 shows the relaxed structures of periclase, α-quartz, and forsterite, indicating the M1 and M2 magnesium positions. An electron density contour plot through a plane in periclase, containing both magnesium and oxygen shows that the material is ionic with the electron density centered on the ions (Figure 1a), in agreement with previous work on MgO[29] and DFT calculations of the electronic structure of CaO, which is isostructural with MgO.[58] In quartz (Figure 1b), two contour plots are shown, one through a plane containing silicon and the other through the parallel plane containing two of the four tetrahedrally coordinating oxygen ions. Bonding in SiO_2 structures is argued to be neither purely ionic nor completely covalent,[66] and we can see from Figure 1b that the electron density in α-quartz is distributed along the Si−O bond, indicating a more covalent character, although more electron density is centered on the oxygen than the silicon, in agreement with density of states calculations by Garvie et al., which suggested considerable polarization of the Si−O bonds.[67] Finally, in forsterite the contour plot is through a plane containing both M1 and M2 magnesium ions. As in periclase, the electron density is centered on the magnesium ions without any density along the Mg−O bond. However, the silica groups resemble quartz, in that the electron density between silicon and oxygen atoms are distributed along the Si−O bonds. The electronic nature of forsterite thus resembles a composite of periclase and quartz, where the Mg−O and Si−O bonds retain their distinctive character. The overall ionicity of the forsterite crystal (where the SiO_4 group can be thought of as a molecular anion) is in agreement with the work by Cohen et al., who found that the nature of the bonding in a hypothetical magnesium silicate perovskite was predominantly ionic.[68] In addition, the covalent nature of the bonding within the SiO_4 group coupled with the ionic bonding between magnesium ions and the SiO_4 groups is very similar to aluminum phosphates, where quantum chemical calculations showed the bonding within the phosphate groups to be covalent in character but ionic between the PO_4 groups and the aluminum ions.[69]

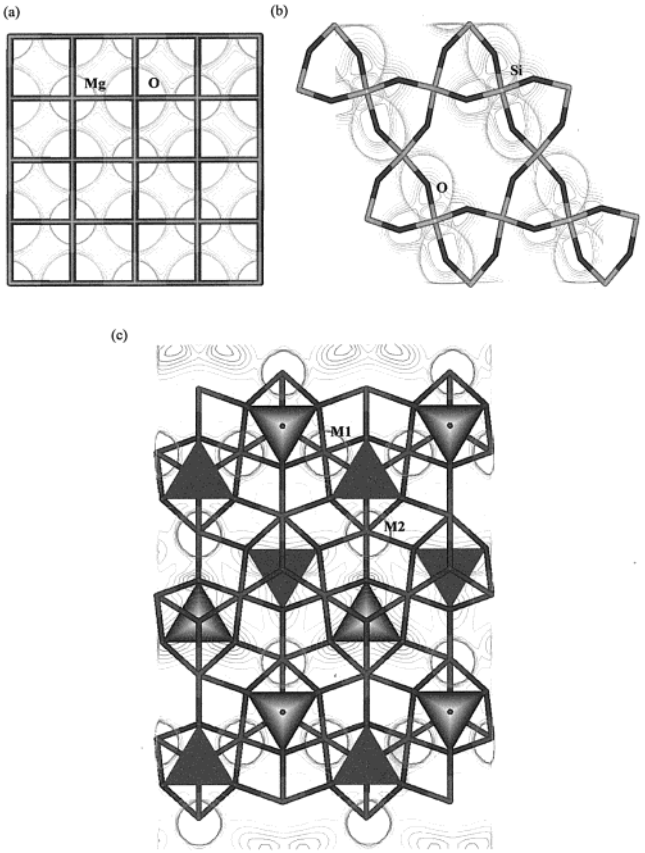

Figure 1. Relaxed structures of (a) periclase, (b) α-quartz, and (c) forsterite with M1 and M2 magnesium sites marked and SiO_4 groups displayed as tetrahedra, showing electron density countour plots through planes containing (a) both Mg and O in periclase, (b) Si and two of the four tetrahedral SiO_4 oxygens in α-quartz, and (c) Mg and two tetrahedral oxygens in forsterite (Mg = mid gray, Si = pale gray, O = dark gray, contour levels are from 0.05 to 0.35 e Å^{-3} at 0.05 e Å^{-3} intervals).

Table 3 lists the calculated energies of the perfect mineral crystals, as well as the various systems containing vacancies and interstitials, which are necessary for the evaluation of the different hydration and protonation processes, discussed in the remainder of this article.

Interstitial Absorption of Water in the Perfect Lattice. We were first interested in investigating the introduction of water molecules interstitially in the perfect mineral lattices. Hence, water molecules were absorbed in the forsterite, periclase, and α-quartz crystals, and the energies were calculated for the process given in the following reaction (in Kroger−Vink notation[70,71]):

$$H_2O_{(g)} \rightarrow H_2O_i^X \quad (1)$$

The absorption energies (from Table 3) are simply

$$E_{(1)} = E3 - (E1 + E8) \quad (2)$$

TABLE 3: Calculated Total Energies of the Lowest Energy Configurations of the Forsterite, α-Quartz, and Periclase Crystals, Together with the Systems Containing Vacancies and Interstitials and Isolated H_2O, H_2, and O_2 Molecules

		calculated (lowest) total energies of crystals and defects (eV)			
no.	calculation	Mg_2SiO_4 bulk	Mg_2SiO_4 {010} surface	α-SiO_2	MgO
E1	perfect lattice	−193.81	−190.20	−573.18	−386.50
E2	stoichiometric unit	−48.45	−47.55	−23.88	−12.08
E3	$(H_2O)_i^X$	−205.56	−220.96 ($2H_2O$)	−677.35 ($8H_2O$)	−395.32
E4	V_{Mg}^x	−183.41 (M1) −182.24 (M2)			−376.66
E5	V_{Si}^x	−173.19		−552.78	
E6	$(2H)_{Mg}^X$	−195.61 (M1) −194.69 (M2)	−196.70 (4H)		−387.87
E7	$(4H)_{Si}^X$	−198.33		−577.83	
E8	$H_2O_{(g)}$	−14.14			
E9	$H_{2(g)}$	−6.80			
E10	$O_{2(g)}$	−7.85			

TABLE 4: Calculated Reaction Enthalpies of the Introduction of Interstitial Gaseous Water Molecules, Magnesium and Silicon Vacancies, Hydrogens at Vacancy Sites, and Replacement of MgO and SiO_2 by Liquid Water Molecules

		calculated reaction enthalpies (kJ mol^{-1})			
equation	reaction	Mg_2SiO_4 bulk	Mg_2SiO_4 {010} surface	α-SiO_2	MgO
1	$H_2O_{(g)} \rightarrow (H_2O)_i^x$	+230	−120	+108	+514
3a	$Mg_{Mg}^x + (1/2)O_2 \rightarrow V_{Mg}^x + MgO_{(s)}$	+217 (M1) +330 (M2)			+163
3b	$Si_{Si}^x + O_2 \rightarrow V_{Si}^x + SiO_{2(s)}$	+443		+421	
5a	$V_{Mg}^x + H_2 \rightarrow (2H)_{Mg}^x$	−521 (M1) −545 (M2)			−425
5b	$V_{Si}^x + 2H_2 \rightarrow (4H)_{Si}^x$	−1112		−1104	
7a	$Mg_{Mg}^x + H_2O_{(l)} \rightarrow (2H)_{Mg}^x + MgO_{(s)}$	+69 (M1) +157 (M2)	−71 (M2)		+111
7b	$Si_{Si}^x + 2H_2O_{(l)} \rightarrow (4H)_{Si}^x + SiO_{2(s)}$	+76		+63	

where E3 is the energy of the crystal with absorbed water molecule, E1 is the energy of the perfect crystal lattice, and E8 is the self-energy of an isolated (gaseous) water molecule. The absorption energies for the different minerals are given in Table 4, from which we can see that the introduction of an interstitial water molecule in the bulk lattices is an endothermic process in all three minerals, but especially in periclase (+513.6 kJ mol^{-1}), where the lattice spacing is too small to allow the easy incorporation of a foreign species such as water. The forsterite crystal has a more open structure than periclase, and it therefore costs much less energy to incorporate a water molecule (Figure 2a). One proton of the (dissociated) water molecule has become bonded to an oxygen atom of a SiO_4 tetrahedron, which has rotated in the crystal lattice. The hydroxyl group has become coordinated to three magnesium ions, at two M1 and one M2 sites.

The α-quartz crystal has a channel structure, more open than either periclase or forsterite, and the lowest energy configuration for the absorbed water molecules occurs when they are accommodated in the channel (Figure 2b). The position of the water molecule's oxygen atom is well away from the central axis of the channel in agreement with ab initio cluster calculations by Fairbrother et al.[72] The calculated absorption energy is only 107.9 kJ mol^{-1} (1.12 eV) which low reaction enthalpy agrees with the fact that α-quartz is well-known to accommodate sizable amounts of water in its lattice.[73] Hagon et al.[42] first calculated the introduction of water molecules in the α-quartz lattice in 1987, but they did not relax the atoms in the lattice, which may explain why they obtained an energy of about 2 eV. Heggie et al.[35] subsequently used classical interatomic potential methods to calculate the same process in a relaxed lattice and obtained an energy for insertion of water into the α-quartz channel of 1.13 eV, whereas Lin et al.[40] used DFT methods within the local density approximation (LDA) to calculate the energy required to introduce an interstitial water molecule into the channel at 0.94 eV. Both values are in excellent agreement with our calculated absorption energy of 1.12 eV.

In addition to incorporating water molecules in the bulk minerals, we investigated the adsorption of water at the forsterite {010} surface, which is the crystal's main cleavage plane. The nondipolar {010} surface is terminated by a layer of oxygen ions and M2 magnesium ions, similar to the main MgO {001} surface. We calculated the adsorption of both molecular and dissociated water molecules at the surface, but found that during the energy minimization of the surface with dissociatively adsorbed water, the water molecules recombined to adsorb associatively onto the surface (shown in Figure 3), indicating that there is no significant energy barrier to the recombination of dissociated water at the surface. Unlike incorporation in the bulk, adsorption of water at the forsterite {010} surface is an exothermic process, which releases 119.8 kJ mol^{-1}.

Introduction of Vacancies. In addition to studying water absorption in the perfect lattice, we were also interested in investigating absorption behavior at cation vacancies in the crystal, which are likely sites for protons dispersed in the lattice to segregate to and form OH groups. For example, Kohn,[38] who used ^1H MAS NMR to study water in forsterite, found evidence of OH groups associated with point defects or as clusters at hydrogarnet type defects (four protons substituting for a silicon ion). However, it has been suggested that at mantle temperatures hydrogens will be present in the mineral as interstitials rather than bound at vacancies[74] and we therefore first needed to calculate the energetics of magnesium and silicon vacancy formation in the three minerals, followed by the adsorption of hydrogen at the vacancies. We were interested in calculating the formation of isolated magnesium and silicon vacancies, rather than the formation of vacancy pairs, and hence, we

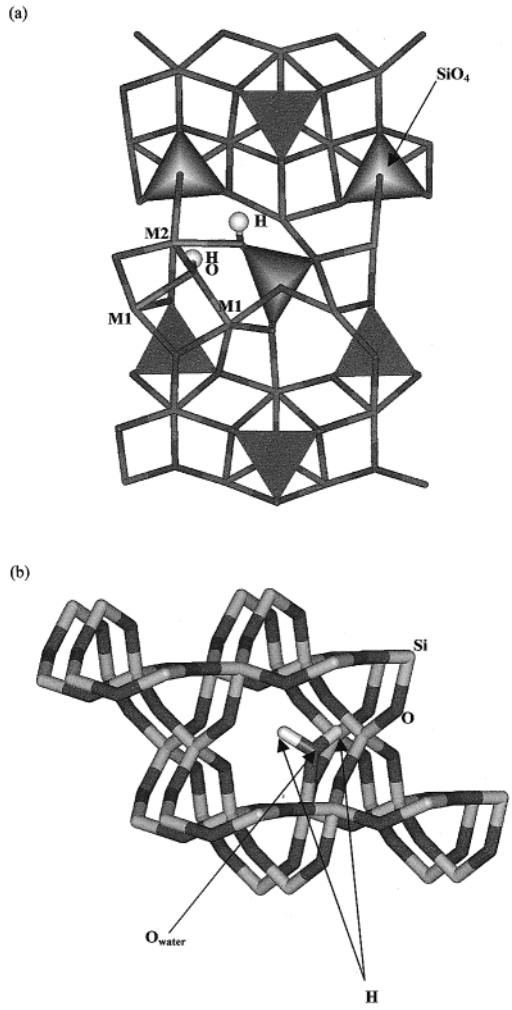

Figure 2. Minimum energy structures of (a) forsterite with absorbed water molecule, showing rotation of SiO_3OH group and coordination of hydroxyl group to three magnesium ions (M1 and M2), and (b) α-quartz, showing a nondissociated interstitial water molecule, coordinated by its oxygen atom to a silicon atom at a position away from the central axis of the channel (Mg = mid gray, Si = pale gray, O = dark gray, and H = white).

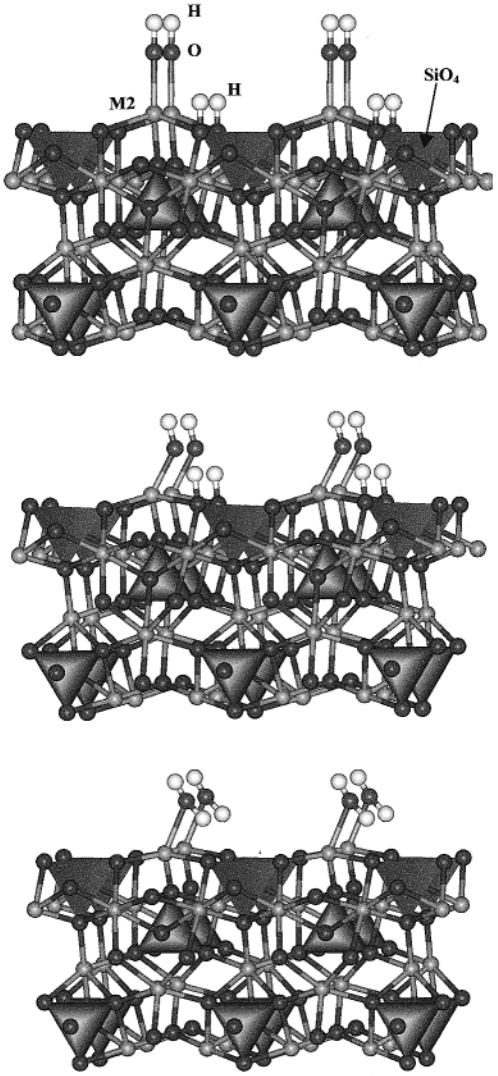

Figure 3. Recombination of dissociatively adsorbed water molecules on the forsterite {010} surface: (a) side view showing initial configuration of a hydroxylated surface; (b) snapshot during minimization process showing tilting of the hydroxyl group and lengthening of $O_{surface}$−H bond; (c) side view of the final configuration showing associatively adsorbed water molecules (Mg = mid gray, Si = pale gray, O = dark gray, and H = white).

calculated the enthalpies of the following reactions:

$$Mg_{Mg}^{X} + \frac{1}{2}O_2 \rightarrow V_{Mg}^{x} + MgO \qquad (3a)$$

and

$$Si_{Si}^{X} + O_2 \rightarrow V_{Si}^{x} + SiO_2 \qquad (3b)$$

From eqs 3a and 3b and Table 3, the energies of Mg and Si vacancy formation respectively are

$$E_{(3a)} = (E2_{(MgO)} + E4) - (E1 + {}^{1}/_{2}E10) \qquad (4a)$$

and

$$E_{(3b)} = (E2_{(SiO2)} + E5) - (E1 + E10) \qquad (4b)$$

where E2 is the energy of the relevant MgO or SiO_2 bulk lattice unit, E4 and E5 are the energies of the crystal containing the vacancy, E1 is the perfect crystal, and E10 is the self-energy of a gaseous oxygen molecule. The calculated vacancy formation energies are then 216.9 and 163.0 kJ mol^{-1} for the removal of a magnesium atom from forsterite (M1) and periclase, respectively, whereas the removal of a silicon atom from forsterite costs 442.6 and 421.2 kJ mol^{-1} from α-quartz. Clearly, it is energetically much more expensive to create a silicon vacancy in the forsterite crystal rather than a magnesium vacancy, and hence, we would expect cation vacancies in the forsterite crystal to be predominantly magnesium vacancies. The larger vacancy formation energies for silicon over magnesium in forsterite are in qualitative agreement with both Wright and Catlow[43] and Brodholt and Refson.[44] Wright and Catlow employed classical interatomic potential methods to investigate vacancy formation in forsteritic olivine. By comparing the energies of defective crystals with the perfect crystal and ions (rather than atoms) at infinity, they calculated energies for the formation of magnesium and silicon vacancies of 24.5 eV (2364 kJ mol^{-1}) and 100.0 eV (9649 kJ mol^{-1}), respectively, whereas they calculated that the formation of cation-oxygen vacancy pairs would cost 8.4 eV (810 kJ mol^{-1}) and 22.5 eV (2168 kJ mol^{-1}) for magnesium and silicon, respectively, in broad agreement with Brodholt and Refson,[44] who used ab initio methods to calculate the formation

of these cation−oxygen vacancy pairs and obtained energies of 7.0 eV (675 kJ mol^{-1}) and 20.3 eV (1959 kJ mol^{-1}) for magnesium and silicon, respectively. Brodholt and Refson[44] suggest that the greater endothermicity of the formation of silicon−oxygen vacancy pairs compared to the magnesium−oxygen vacancy pairs is due to the greater charge of the silicon vacancy rather than the necessity of creating two oxygen vacancies for each silicon vacancy as compared to one oxygen vacancy per magnesium. Our calculations bear out their suggestion as no oxygen vacancies are created in our calculation and the ratio of the energies of formation of magnesium vacancies to silicon vacancies is approximately Mg:Si = 1:2, i.e., the ratio of their formal charges. However, our calculated energies of neutral vacancy formation are much less endothermic than either charged vacancy formation, using the approach of removing the defect ion from the lattice to infinity,[43] or cation-oxygen vacancy pair formations,[44] and hence appears a reasonable route to the formation of point defects in the crystal, where interstitial hydrogens can segregate to and combine with the low-coordinated oxygen atoms to form OH clusters, which are observed experimentally in forsterite.[38]

Protonation of Magnesium and Silicon Vacancies. Hence, we next studied the process of incorporating hydrogens at the cation vacancies in the three minerals, namely

$$V_{Mg}^{x} + H_2 \rightarrow (2H)_{Mg}^{x} \quad (5a)$$

in forsterite and periclase and

$$V_{Si}^{x} + 2H_2 \rightarrow (4H)_{Si}^{x} \quad (5b)$$

in α-quartz and forsterite. The energies of these processes (given in Table 4) are calculated from Table 3 as follows:

$$E_{(5a)} = E6 - (E4 + E9) \quad (6a)$$

and

$$E_{(5b)} = E7 - (E5 + 2\,E9) \quad (6b)$$

where E4 and E5 as before are the energies of the crystals containing cation vacancies, E9 is the self-energy of a gaseous H_2 molecule, and E6 and E7 are the minerals with protons incorporated at the cation vacancy site. It is clear from Table 4 that hydrogen adsorption at the cation vacancies is a highly exothermic process in all three materials but especially at the silicon vacancies in both quartz and forsterite. However, the average enthalpy of adsorption per hydrogen atom falls in a fairly narrow range of −212 to −278 kJ mol^{-1}, although it is still energetically more favorable to adsorb at a silicon vacancy (∼ −277 kJ mol^{-1}) than at a magnesium vacancy (∼ −236 kJ mol^{-1}). The enthalpy of reaction 5a is lower for periclase than for forsterite, which added to the smaller heat of formation of the magnesium vacancy in periclase (3a) indicates that magnesium vacancies are more stable in periclase than in forsterite. The enthalpy of reaction 5b is very similar for forsterite and quartz and so is the energy of formation of silicon vacancies in both minerals (3b). Hence, the stability of silicon vacancies in both materials are comparable, probably because both the silicon geometry in the lattice, as the center of four tetrahedrally coordinated oxygen atoms, and the electron density distributions (Figure 1 parts b and c) round the oxygen and silicon atoms in forsterite and quartz are very similar. The electron density distribution round the magnesium ion in both periclase and forsterite is also similar but not that surrounding the oxygen ion, which in forsterite is not only bonded to three magnesium atoms, but also more covalently to one silicon. In periclase, on the other hand, each oxygen atom is bonded to six magnesium ions in octahedral coordination. In addition, the geometry of the cation, and the subsequent vacancy site, is different in both minerals. Periclase is a much more closely packed structure than forsterite, and the vacancy site is smaller, which may explain the lower exothermicity of introducing two protons at the vacancy site in periclase.

Dissolution of MgO and SiO_2 Units. Cation dissolution is often one of the first steps in mineral dissolution processes, and hence, we were interested in modeling this initial stage in the dissolution process by calculating the replacement of MgO and SiO_2 units by one and two water molecules, respectively. The net effect of the calculation is replacement of cations by protons, the sum of the processes described in eqs 3 and 5, but as dissolution processes take place in an aqueous environment we calculate the process not with respect to gaseous O_2 and H_2 but with respect to liquid water, adding the experimental energy of condensation of water[75] of −44 kJ mol^{-1} to the calculated self-energy of gaseous water molecules (E8 in Table 3). We thus calculate the processes given in the following reactions:

$$Mg_{Mg}^{x} + H_2O_{(l)} \rightarrow (2H)_{Mg}^{x} + MgO_{(s)} \quad (7a)$$

and

$$Si_{Si}^{x} + 2H_2O_{(l)} \rightarrow (4H)_{Si}^{x} + SiO_{2(s)} \quad (7b)$$

where the reaction enthalpies (Table 4) are calculated from Table 3 as follows:

$$E_{(7a)} = E2 + E6 - E1 - (E8 - 44.0\ \text{kJ mol}^{-1}) \quad (8a)$$

and

$$E_{(7b)} = E2 + E7 - E1 - (E8 - 44.0\ \text{kJ mol}^{-1}) \quad (8b)$$

The replacement of both magnesium and silicon from the bulk crystal is an endothermic process in all three minerals. In the case of magnesium, the replacement enthalpy for periclase (111 kJ mol^{-1}) falls between those for the two different magnesium sites in forsterite (69 and 157 kJ mol^{-1} for the M1 and M2 sites, respectively), whereas the enthalpies for the silicon process are again very similar for forsterite and quartz, indicating once more that these enthalpies are determined more by geometry rather than by electronic effects. Figure 4a shows the bulk forsterite crystal with SiO_2 unit replaced by two water molecules (which structure is of course identical to the crystal with one silicon atom replaced by four hydrogens). The lattice surrounding the defect is not distorted, as it is when a water molecule was introduced in the perfect lattice (Figure 2a). The four protonated oxygen atoms still lie at the corners of a tetrahedron, whereas three of the four protons point in the direction of the silicon vacancy at the center of the tetrahedron. However, the fourth proton is directed away from the tetrahedral center, similar to the structure found by Brodholt and Refson.[44] Catlow and co-workers[37,43] calculated the replacement of magnesium by two protons in both periclase and forsterite using interatomic potential methods. They obtained energies of 5.81 eV (560 kJ mol^{-1}) and 3.71 eV (358 kJ mol^{-1}) for periclase and forsterite, respectively. These energies are of course much larger than ours, which may be due to lesser electronic polarization in the interatomic potential method, which is generally seen when DFT calculations and interatomic potential

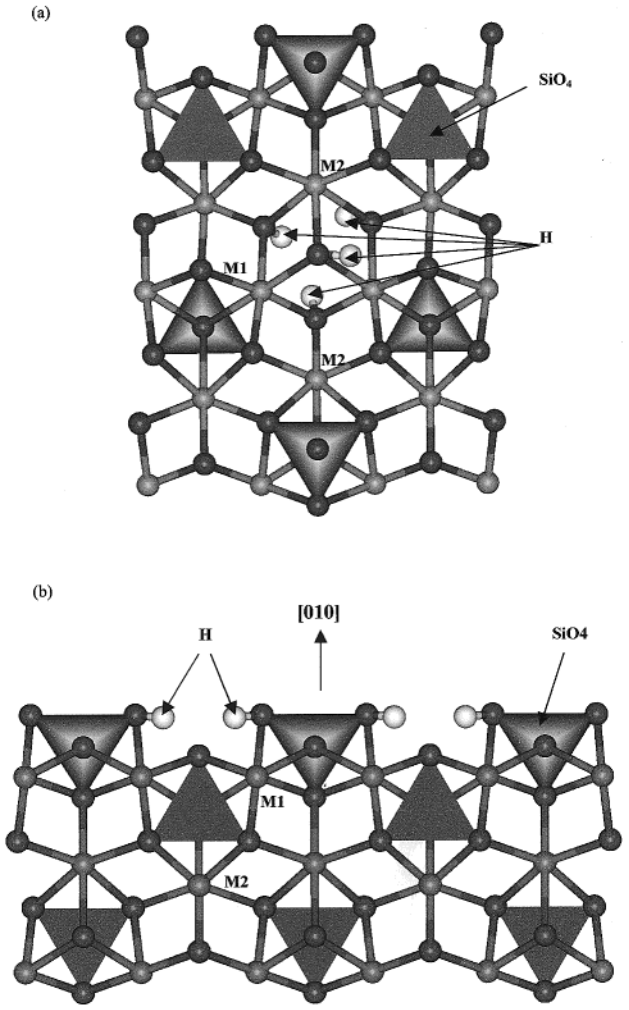

Figure 4. Minimum energy structure of (a) bulk forsterite with one silicon ion replaced by four hydrogens, showing negligible distortion of the lattice with three hydrogen atoms directed toward the Si vacancy, and (b) the forsterite {010} surface with two magnesium ions replaced by two hydrogens each, both pointing toward the Mg vacancy.

calculations are compared,[58] or to the fact that they have used an estimation for the energy of dissocation of the water molecule.[43] As we know from experimental evidence[38] that water is present in significant quantities in the forsterite mineral, their energies seem rather large, and we would suggest that the energies obtained in this present study are more realistic, even though perhaps somewhat on the low side. Brodholt and Refson[44] also calculated the process in forsterite with respect to gaseous water molecules, using DFT methods, and obtained energies of 0.6 eV (58 kJ mol^{-1}) and −0.24 eV (−23 kJ mol^{-1}) for the M1 magnesium and silicon atoms, respectively. If we consider the reaction with gaseous water instead of liquid water, our replacement energies are calculated at +0.26 and −0.12 eV for M1 magnesium and silicon, respectively, which is in good agreement with their calculated energies.

Although cation leaching from the bulk materials is, not surprisingly, an energetically unfavorable process, when we replace the (M2) magnesium ions by two protons each at the {010} surface of forsterite, the reaction is exothermic by approximately 71 kJ mol^{-1}, in qualitative agreement with Grandstaff[76] who measured a negative standard free energy and enthalpy change for the proton-promoted surface dissolution of magnesium-rich olivine[77] and experimental work by Ghazy et al. on leaching of Mg ions from olivine surfaces at low pH.[78]

Figure 4b shows the relaxed structure of the forsterite {010} surface with surface M2 magnesium ions replaced by two protons each, both of which are pointing toward the magnesium vacancy.

Conclusion

We employed electronic structure calculations to investigate the absorption of water in forsterite, periclase, and α-quartz. The calculated structural parameters of the three minerals are in good agreement with the experimental structure.

Absorbing gaseous water molecules in the perfect lattices of forsterite, periclase, and α-quartz leads to distortion of the periclase and forsterite lattices and is calculated to be an endothermic process in all three materials, more so in periclase and forsterite than in α-quartz. In α-quartz, the calculated absorption energy and geometry of the interstitial water molecule in the channel agree with previous modeling studies using different computational techniques.

Adsorption of water at the forsterite {010} surface is energetically favorable. Water is found to adsorb associatively onto the surface, and there is no energy barrier to recombination of dissociatively adsorbed water molecules.

The introduction of neutral magnesium and silicon vacancies into the mineral lattices is an endothermic process in all three materials. Magnesium vacancy formation is energetically less expensive than the formation of silicon vacancies, which are found to be similar in energy in both quartz and forsterite, probably due to the similar structural and electronic nature of the silicon sites in both materials. Introduction of a magnesium vacancy in periclase is less endothermic than in forsterite, probably due to the different nature of the magnesium (and oxygen) sites in these two materials. Although the energies of silicon vacancy formation in forsterite are high (443 kJ mol^{-1}), the formation of a magnesium vacancy in forsterite is calculated to cost about 217 kJ mol^{-1}, which may not be an insurmountable energy barrier at elevated temperatures.

The subsequent absorption of hydrogens at the magnesium and silicon vacancies is a highly exothermic process, on average releasing more energy per hydrogen atom absorbed at the silicon vacancies than at the magnesium defects. Replacement of magnesium and silicon atoms by liquid water molecules, as a first step in the mineral dissolution process, is found to be an endothermic process in the bulk materials but exothermic when replacing magnesium ions on the forsterite {010} surface, in agreement with experiment.

Acknowledgment. N.H.dL. thanks professors C.R.A. Catlow and S.C. Parker for useful discussions, NERC, Grant No. GR3/11779, for financial support, and the Mineral Physics and Materials Consortia for the provision of computer time on the Cray T3E.

References and Notes

(1) Dana, E. S. *A Textbook of Mineralogy*; John Wiley & Sons, Inc.: New York, 1941.

(2) Mitchell, M. B. D.; Jackson, D.; James, P. F. *J. Non-Cryst. Solids* **1998**, *225*, 125.

(3) Dubrovinskaya, N. A.; Dubrovinsky, L. S.; Saxena, S. K. *Geochim. Cosmochim. Acta* **1997**, *61*, 4151.

(4) Kerschhofer, L.; Sharp, T. G.; Rubie, D. C. *Science* **1996**, *274*, 79.

(5) Purton, J. A.; Allan, N. L.; Blundy, J. D.; Wasserman, E. A. *Geochim. Cosmochim. Acta* **1996**, *60*, 4977.

(6) Purton, J. A.; Allan, N. L.; Blundy, J. D. *Geochim. Cosmochim. Acta* **1997**, *61*, 3927.

(7) Hirth, G.; Kohlstedt, D. L. *J. Geophys. Res. Solid Earth* **1995**, *100*, 1981.

(8) Kohlstedt, D. L.; Zimmerman, M. E. *Annu. Rev. Earth Planet. Sci*. **1996**, *24*, 41.
(9) Deer, W. A.; Howie, R. A.; Zussman, J. *Introduction to the rock-forming minerals*, 2nd ed.; Longman: Essex, U.K., 1992.
(10) Hickel, P. E.; Lafon, F.; Fortis, F.; Cambon, O.; Demazeau, G. *Annal. Chim. Sci. Mater*. **1997**, *22*, 571.
(11) Hickel, P. E.; Lafon, F.; Chvansky, P. P.; Largetreau, A.; Demazeau, G. *Annal. Chim. Sci. Mater*. **1997**, *22*, 583.
(12) Balascio, J. F.; Lind, T. *Curr. Opin. Solid State Mater. Sci*. **1997**, *2*, 588.
(13) Lee, K. J.; Seo, K. W.; Yu, H. S.; Mok, Y. I. *Korean J. Chem. Eng.* **1996**, *13*, 489.
(14) Arnaud, R.; Cambon, O. *Annal. Chim. Sci. Mater*. **1997**, *22*, 577.
(15) Lafon, F.; Demazeau, G. *J. Phys. IV* **1994**, *4C2*, 177.
(16) de Leeuw, N. H.; Higgins, F. M.; Parker, S. C. *J. Phys. Chem. B* **1999**, *103*, 1270.
(17) Krauskopf, K. B.; Bird, D. K. *Introduction to Geochemistry*, 3rd ed.; McGraw-Hill, Inc.: New York, 1995; Chapter 16.
(18) Langel, W.; Parrinello, M.; *Phys. Rev. Lett*. **1994**, *73*, 504.
(19) Wu, M.-C.; Estrada, C. A.; Corneille, J. L.; Goodman, D. W. *J. Chem. Phys*. **1992**, *96*, 3892.
(20) Li, C.; Li, G.; Xin, Q. *J. Phys. Chem*. **1994**, *98*, 1933.
(21) Henrich, V. *Surf. Sci*. **1976**, *57*, 385.
(22) Coluccia, S.; Tench, A. J.; Segall, R. L. *J. Chem. Soc., Faraday Trans. 1* **1979**, *75*, 1769.
(23) Varma, S.; Chen, X.; Zhang, J.; Davoli, I.; Saldin, D. K.; Tonner, B. P. *Surf. Sci*. **1994**, *314*, 145.
(24) Jordan, G.; Higgins, S. R.; Eggleston, C. M. *Am. Mineral*. **1999**, *84*, 144.
(25) Tasker, P. W.; Colbourn, E. A.; Mackrodt, W. C. *J. Am. Ceram. Soc*. **1985**, *68*, 74.
(26) Matsui, M. *J. Chem. Phys*. **1989**, *91*, 489.
(27) Gibson, A.; Haydock, R.; LaFemina, J. P. *Phys. Rev. B* **1994**, *50*, 2582.
(28) Watson, G. W.; Kelsey, E. T.; de Leeuw, N. H.; Harris, D. J.; Parker, S. C. *J. Chem. Soc., Faraday Trans.* **1996**, *92*, 433.
(29) Kantorovich, L. N.; Holender, J. M.; Gillan, M. J. *Surf. Sci*. **1995**, *343*, 221.
(30) Shalabi, A. S.; El-Mahdy, A. M. *Phys. Lett. A* **2001**, *281*, 176.
(31) Pugh, S.; Gillan, M. J. *Surf. Sci*. **1994**, *320*, 331.
(32) Refson, K.; Wogelius, R. A.; Fraser, D. G.; Payne, M. C.; Lee, M. H.; Milman, V. *Phys. Rev. B* **1995**, *52*, 10823.
(33) Szymanski, M. A. *Surf. Sci*. **1996**, *367*, 135.
(34) Mejias, J. A.; Refson, K.; Fraser, D. G. *Chem. Phys. Lett*. **1999**, *314*, 558.
(35) Heggie, M. I.; Jones, R.; Latham, C. D.; Maynard, S. C. P.; Tole, P. *Philos. Magn. B* **1992**, *65*, 463.
(36) Reuschle, T.; Darot, M. *Eur. J. Mineral*. **1996**, *8*, 695.
(37) Catlow, C. R. A.; Baram, P. S.; Parker, S. C.; Purton, J.; Wright, K. V. *Philos. Trans. R. Soc. London A* **1995**, *350*, 265.
(38) Kohn, S. C. *Am. Mineral*. **1996**, *81*, 1523.
(39) Purton, J.; Jones, R.; Heggie, M.; Oberg, S.; Catlow, C. R. A. *Phys. Chem. Miner*. **1992**, *18*, 389.
(40) Lin, J. S.; Payne, M. C.; Heine, V.; McConnell, J. D. C. *Phys. Chem. Miner*. **1994**, *21*, 150.
(41) Jones, R.; Oberg, S.; Heggie, M. I.; Tole, P. *Philos. Mag. Lett*. **1992**, *66*, 61.
(42) Hagon, J. P.; Stoneham, A. M.; Jaros, M. *Philos. Mag. B* **1987**, *55*, 225.
(43) Wright, K.; Catlow, C. R. A. *Phys. Chem. Miner*. **1994**, *20*, 515.
(44) Brodholt, J. P.; Refson, K. *J. Geophys. Res. Solid Earth* **2000**, *105*, 18977.
(45) Watson, G. W.; Oliver, P. M.; Parker, S. C. *Phys. Chem. Miner*. **1997**, *25*, 70.
(46) de Leeuw, N. H.; Parker, S. C.; Catlow, C. R. A.; Price, G. D. *Phys. Chem. Miner*. **2000**, *27*, 332.
(47) Kresse, G.; Hafner, J. *Phys. Rev. B* **1993**, *47*, 5858.
(48) Kresse, G.; Hafner, J. *Phys. Rev. B* **1994**, *49*, 14251.
(49) Kresse, G.; Furthmüller, J. *Comput. Mater. Sci.* **1996**, *6*, 15.
(50) Kresse, G.; Furthmüller, J. *Phys. Rev. B* **1996**, *54*, 11169.
(51) Bates, S. P.; Kresse, G.; Gillan, M. J. *Surf. Sci*. **1998**, *409*, 336.
(52) Vanderbilt, D. *Phys. Rev. B* **1990**, *41*, 7892.
(53) Jones, R.; Gunnarsson, O. *Rev. Mod. Phys*. **1989**, *61*, 689.
(54) Payne, M.; Teter, M.; Allan, D.; Arias, T.; Joannopoulos, *J. Rev. Mod. Phys*. **1992**, *64*, 1045.
(55) Gillan, M. *Contemp. Phys*. **1997**, *38*, 115.
(56) Kresse, G.; Hafner, J. *Phys. Rev. B* **1993**, *48*, 13115.
(57) Schroer, P.; Kruger, P.; Pollman, J. *Phys. Rev. B* **1994**, *49*, 17092.
(58) de Leeuw, N. H.; Purton, J. A. *Phys. Rev. B* **2001**, *63*, 195417.
(59) Perdew, J. P.; Chevary, J. A.; Vosko, S. H.; Jackson, K. A.; Pederson, M. R.; Singh, D. J.; Fiolhas, C. *Phys. Rev. B Condens. Matter* **1992**, *46*, 6671.
(60) Monkhorst, H. J.; Pack, J. D. *Phys. Rev. B* **1976**, *13*, 5188.
(61) Smyth, J. R.; Hazen, R. M. *Am. Mineral*. **1973**, *58*, 588.
(62) Liu, F.; Garofalini, S. H.; King-Smith, R. D.; Vanderbilt, D. *Phys. Rev. B* **1994**, *49*, 12528.
(63) Keskar, N. R.; Chelikowsky, J. R. *Phys. Rev. B* **1992**, *46*, 1.
(64) Teter, D. M.; Gibbs, G. V.; Boisen, M. B., Jr.; Allan, D. C.; Teter, M. P. *Phys. Rev. B* **1995**, *52*, 8064.
(65) Königstein, M.; Corà, F.; Catlow, C. R. A. *J. Solid State Chem*. **1998**, *137*, 261.
(66) Catlow, C. R. A.; Price, G. D. *Nature* **1990**, *347*, 243.
(67) Garvie, L. A. J.; Rez, P.; Alvarez, J. R.; Buseck, P. R.; Craven, A. J.; Brydson, R. *Am. Mineral*. **2000**, *85*, 732.
(68) Cohen, R. E.; Boyer, L. L.; Mehl, M. J.; Pickett, W. E.; Krakauer, H. *Perovskites*; American Geophysical Union: Washington, DC, 1988.
(69) Corà, F.; Catlow, C. R. A.; d'Ercole, A. *J. Mol. Catal. A: Chem*. **2001**, *166*, 87.
(70) Kroger, F. A.; Vink, V. J. *Solid State Physics*; Academic Press: New York, 1956; Vol. 3, p 307.
(71) Kingery, W. D.; Bowen, H. K.; Uhlmann, D. R. *Introduction to ceramics*; Wiley: New York, 1976; p 127.
(72) Fairbrother, P.; Heggie, M. I.; Jones, R.; Tole, P.; Oberg, S. *Mater. Res. Soc. Symp. Proc.* **1990**, *193*, 271.
(73) Griggs, D. T.; Blacic, J. D. *Science* **1965**, *147*, 292.
(74) Haiber, M.; Ballone, P.; Parrinello, M. *Am. Mineral*. **1997**, *82*, 913.
(75) Johnson, D. A. *Some thermodynamic aspects of inorganic chemistry*; Cambridge University Press: Cambridge, U.K., 1982.
(76) Grandstaff, D. E. In *Rates of Chemical Weathering of Rocks and Minerals*; Colman, S. M., Dethier, D. P., Eds.; Academic Press, Inc.: New York, 1981; p 41.
(77) Wieland, E.; Wehrli, B.; Stumm, W. *Geochim. Cosmochim. Acta* **1988**, *52*, 1969.
(78) Ghazy, S. E.; Kabil, M. A.; Abeidu, A. M.; El-Metwally, N. M. *Sep. Sci. Technol*. **1996**, *31*, 829.